Eur. Phys. J. D **15**, 65–77 (2001)

THE EUROPEAN PHYSICAL JOURNAL D

EDP Sciences

Some new properties of deformed atomic clusters described in a projected spherical basis

A.A. Raduta[1,2,3,a], E. Garrido[3], and E. Moya de Guerra[3]

[1] Department of Theoretical Physics, Bucharest University, Bucharest, POB MG11, Romania
[2] Institute of Physics and Nuclear Engineering, Bucharest, POB MG6, Romania
[3] Instituto de Estructura de la Materia, CSIC, Serrano 119-123, 28006 Madrid, Spain

Received 28 November 2000 and Received in final form 15 February 2001

Abstract. Some properties of small sodium clusters, comprising up to 45 atoms, are described using a projected spherical single particle basis. The variation of the cluster shape and inner density with the number of atoms is studied. Seemingly chestnut, clusterization and halo like structures are identified for several metallic clusters. Static polarizabilities and plasmon frequencies are calculated and compared with experimental data and with results obtained in different approaches.

PACS. 36.40.-c Atomic and molecular clusters – 73.20.Mf Collective excitations (including excitons, polarons, plasmons and other charge-density excitations)

1 Introduction

Although it is very old, the field of metallic cluster has been reinforced in 1984 by the pioneering paper of Knight *et al.* [1] pointing out the electronic shells in alkali-metallic clusters. Since that time many works have been performed on both theoretical and experimental sides. The notable contributions in the new era of the field have been reviewed by several papers in the last decade [2–4].

The most interesting category of clusters seems to be those with a moderate number of atoms. Indeed for such systems neither statistical models [5] nor *ab initio* quantum-chemical methods [6] are justified. Instead the mean field approach is vastly used. Several solutions defining the mean field for the single particle motion have been employed along the years. Among them, three procedures are to be distinguished: (i) solving the Kohn-Sham equations [7], (ii) assuming that the positive charge of the ionic core is uniformly distributed in a sphere of radius R. This is known in the literature as jellium hypothesis [8,9], (iii) postulating the average potential [10].

Since the shell structure and magic numbers are associated to the spherical symmetry, the spherical clusters have been intensively studied. However there are some features like the detailed structure of the abundance spectrum [11], or the split of plasmon energies [12–14], which cannot be explained assuming a spherical symmetry for the mean field. The first paper devoted to the deformed clusters was due to Clemenger and published in 1985 [15]. The author adapts the Nilsson model formulated for nuclear systems [16], by ignoring the spin-orbit term. The resulting model is referred to as Clemenger-Nilsson (CN) model. The CN model was very successful in explaining several properties which depend on the shape of the cluster and which could not be described within a formalism using a mean field with spherical symmetry. The model is suitable to describe the single particle properties in the intrinsic frame and especially for strong coupling regime when the wave function of the whole system can be factorized into an intrinsic part and a Wigner function accounting for the rotational degrees of freedom. However there are many properties which are very sensitive to the change of angular momentum of the system. Moreover in most cases "K" is not a good quantum number and therefore the factorization mentioned above is not possible. The typical case of this kind is that of systems of triaxial shape. A many body treatment of such situations would require a subsequent projection of the angular momentum. However such operation is technically very difficult to be achieved and to our knowledge up to now only approximative solutions have been proposed. In a previous publication, one of us (A.A.R.) proposed a solution for constructing a single particle basis with good spherical symmetry and depending on deformation [17]. Before being used in an RPA (random phase calculations) approach, the model should be tested for pointing its ability to account in a realistic fashion for the main features of the deformed clusters. Thus, in reference [17] the cluster shape, the magic numbers, and super-shell effects have been determined and a good agreement with the data as well as with the previous theoretical results have been obtained.

[a] e-mail: raduta@theor1.theory.nipne.ro
or e-mail: raduta@ifin.nipne.ro

The aim of the present paper is to continue the exploration of the cluster properties within the projected spherical basis introduced in reference [17]. The specific structure of the single particle wave functions should be reflected in the charge distribution of the valence electrons. This structure might be important when one wants to investigate the response of the cluster to the action of an external electromagnetic field. In reference [18], a parallel study of nuclear systems and atomic clusters has been performed and the conclusion was that the two systems have many similar properties. Studies of momentum distributions in reference [19] also show such a parallelism. In this context we find worthwhile looking for satellite clusters with skin structure, empty center, hard center, cluster subsystems and halo behavior. Such properties might be seen in the structure of the density function. If these structures are identified then another questions deserves attention namely whether they manifest themselves when the cluster interacts with an external electromagnetic field.

The project sketched above is accomplished according to the following plan. In Section 2 a brief review of the theoretical model of reference [17] is presented. The valence electron density is studied in Section 3. The cluster spatial extension is investigated in Section 4 by calculating the root mean square (r.m.s.) radii. The static polarizabilities and plasmon frequencies are calculated in Section 5. The final conclusions are drawn in Section 6.

2 The mean field and the projected spherical basis

We restrict our considerations to the energy domain of laser beam experiments (*i.e.* optical domain) where only the valence electrons may be excited and de-localized, the remaining ones defining the atomic core. Under these circumstances we could study those atomic cluster properties which are mainly determined by the valence electrons. The picture is even more simplified if the cluster building block is an alkali-metal. In this case the interacting system of electrons and positively charged ions is replaced by a system of interacting electrons moving in a mean field which accounts for the influence of the ionic core on the single particle motion. Each atom of a given cluster is represented by one valence electron.

In a previous publication [17], the mean field for the valence electrons is defined with the help of a model Hamiltonian associated to the particle-core interacting system

$$\begin{aligned} H_{\rm pc} &= \frac{p^2}{2m_{\rm e}} + \frac{m_{\rm e}\omega_0^2 r^2}{2} + D\left(l^2 - \langle l^2\rangle\right) \\ &\quad + H_{\rm c} - m_{\rm e}\omega_0^2 r^2 \sum_{\lambda=0,2} \sum_{-\lambda\le\mu\le\lambda} \alpha^*_{\lambda\mu} Y_{\lambda\mu} \\ &\equiv H_{\rm p} + H_{\rm c} + H_{\rm int}, \end{aligned} \tag{2.1}$$

where $\alpha_{\lambda\mu}$ are shape variables defining the deformed ionic core through the surface equation:

$$R = R_0\left(1 + \sum_{\lambda=0,2} \sum_{-\lambda\le\mu\le\lambda} \alpha^*_{\lambda\mu} Y_{\lambda\mu}\left(\theta,\phi\right)\right). \tag{2.2}$$

The parameters defining $H_{\rm p}$ are the same as in reference [15], *i.e.* $D = -0.04\hbar\omega_0$ and $\hbar\omega_0 = E_{\rm F}\mathcal{N}^{-\frac{1}{3}}$ with $E_{\rm F}$ and $\mathcal{N}$ standing for the Fermi energy and the number of atoms. The volume conservation condition allows us to relate the monopole and quadrupole coordinates [17]. The shape coordinates $\alpha_{2\mu}$ and their conjugate momenta define the boson operators $b^+_{2\mu}$ associated to the harmonic vibration of the core:

$$\begin{aligned} \alpha_{2\mu} &= \frac{1}{k\sqrt{2}}\left(b^+_{2\mu} + (-)^\mu b_{2-\mu}\right); \\ \pi_{2\mu} &= \frac{{\rm i}k}{\sqrt{2}}\left(-b_{2\mu} + (-)^\mu b^+_{2-\mu}\right). \end{aligned} \tag{2.3}$$

The above canonical transformation is determined up to a constant k. The term describing the core is:

$$H_{\rm c} = \omega_{\rm c} \sum_{-2\le\mu\le2} b^\dagger_{2\mu} b_{2\mu}, \tag{2.4}$$

while the single particle Hamiltonian $H_{\rm p}$ is just the spherical shell model operator from which we omit, as usual, the spin-orbit term. Note that $H_{\rm pc}$ (Eq. (2.1)) is invariant to rotations performed in the product space of the particle and core states.

Let us consider the coherent state

$$|\Psi_{\rm c}\rangle = \exp\left(d\left(b^+_{20} - b_{20}\right)\right)|0\rangle, \tag{2.5}$$

where $|0\rangle$ and d are used to denote the quadrupole boson vacuum and a real parameter simulating the quadrupole deformation, respectively. Averaging $H_{\rm pc}$ on the coherent state (2.5) one obtains, a deformed single particle Hamiltonian which is, up to an additive constant, similar to the Nilsson-Clemenger Hamiltonian

$$\langle\Psi_{\rm c}|H_{\rm pc}|\Psi_{\rm c}\rangle \equiv H^{(d)}_{\rm p} \approx H_{\rm NC}. \tag{2.6}$$

The volume conservation condition determines a monopole term in the single particle Hamiltonian $H^{(d)}_{\rm p}$. The Hamiltonians $H^{(d)}_{\rm p}$ and $H_{\rm NC}$ have the same functional dependence on spatial coordinates. However they differ from each other by the coefficients determining the strength of the deformation. We require that the average of the $\alpha^*_{2\mu}Y_{2\mu}$ term in the particle-core Hamiltonian is identical to the deformed single particle potential from the Clemenger Hamiltonian. This provides an equation relating the deformation parameters δ and d in the Nilsson-Clemenger and the present models, respectively:

$$d = k\sqrt{\frac{2\pi}{45}}(\Omega_\perp^2 - \Omega_z^2) \tag{2.7}$$

with:

$$\Omega_\perp = \left(\frac{2+\delta}{2-\delta}\right)^{1/3},\ \Omega_z = \left(\frac{2+\delta}{2-\delta}\right)^{-2/3}. \tag{2.8}$$

The state $\Psi_{\rm c}$ describes the ground state of a deformed quadrupole boson Hamiltonian

$$H_{\rm c}^{(d)} = \omega_{\rm c}\left[\sum_\mu b_{2\mu}^+ b_{2\mu} - d\left(b_{20}^+ + b_{20}\right) + d^2\right]. \tag{2.9}$$

We could define a coherent state for the particle motion $\Psi_{\rm p}$ so that the corresponding average of $H_{\rm pc}$ is the boson operator $H_{\rm c}^{(d)}$.

Concluding, the averaging operation on coherent states breaks the rotational symmetries since some dynamical variables are frozen at their static values. This suggests a mechanism of restoring the rotational symmetry in the space of single particle states. One could use the eigenstates of the particle core Hamiltonian for treating the single particle motion. In this case the matrix elements for the operators acting on particle degrees of freedom are obtained by integrating first over the core variables which results in overlapping the core components of the wave function. Instead, in reference [17], a simpler way of treating the deformed single particle mean field was presented. Indeed, through a projection method, a set of orthogonal states having spherical symmetry was defined:

$$\begin{aligned}\phi_{IM;\sigma}(nl;d) &= \mathcal{N}_{nl}^I(d)\left[P_{MI}^I|nlI\rangle\Psi_{\rm c}(d)\right]\chi_\sigma,\\ &\text{for } I\neq 0,\ l=\text{even}\\ \phi_{00;\sigma}(nl;d) &= \mathcal{N}_{nl}^0(d)\left[P_{00}^0\left[|nl\rangle\hat{s}\right]_{l+1,0}\Psi_{\rm c}(d)\right]\chi_\sigma,\\ &\text{for } I=0,\ l=\text{odd}\end{aligned} \tag{2.10}$$

where P_{MK}^I denotes the angular momentum projection operator and $\mathcal{N}_{nl}^I(d)$ the norm of the projected state. For the state with $I=0, l=$ odd, the use of the spin operator $\hat{s}$ to construct a state of good angular momentum is necessary. The standard notation for the spherical shell model state is used:

$$|nlM\rangle\chi_\sigma = R_{nl}Y_{lM}\chi_\sigma. \tag{2.11}$$

These functions might approximate the eigenfunctions of $H_{\rm pc}$ obtained through diagonalization in the basis $\left[|nl\rangle\phi_J^{(\rm c)}\right]_{IM}\chi_\sigma$, with $\phi_{JM}^{(\rm c)}$ denoting the state of good quantum numbers J, M, projected out the state $\Psi_{\rm c}(d)$ describing the deformed core. Moreover, according to the arguments mentioned before, they approximate the states of good angular momentum projected from the eigenstates of $H_{\rm p}^{(d)}$.

If one neglects the matrix elements with $\Delta l = \pm 2$ and $\Delta n = 2$ the eigenvalues of $H_{\rm pc}$ within the projected spherical basis can be fairly well approximated by the average values:

$$\begin{aligned}\epsilon_{nl}^I(d) &\equiv \langle\phi_{IM;\sigma}(nl;d)|H|\phi_{IM;\sigma}(nl;d)\rangle\\ &= \hbar\omega_0\left(N+\frac{3}{2}\right) + D\left[l(l+1) - \frac{N(N+3)}{2}\right]\\ &+\hbar\omega_0\left(N+\frac{3}{2}\right)\frac{1}{90}\left(\Omega_\perp^2 - \Omega_z^2\right)^2\\ &\times\left[1+\frac{1}{d^2}\Big\langle\sum_\mu b_{2\mu}^+ b_{2\mu}\Big\rangle\right]\\ &-\hbar\omega_0\left(N+\frac{3}{2}\right)\frac{1}{3}\left(\Omega_\perp^2 - \Omega_z^2\right)F_{Il}.\end{aligned} \tag{2.12}$$

where F_{Il} is a geometric factor given in reference [17][1].

To conclude, in our model the Hamiltonian for the single particle motion is $H_{\rm p}^{(d)}$. Its eigenvalues are approximated by $\epsilon_{nl}^I(d)$ given by the equation (2.12) while a subset of projected spherical eigenstates is described by the orthogonal basis defined by (2.10). How the particle operators are treated in the space of projected states, is explained in detail in reference [17]. As shown there, the space spanned by the projected states $\{\phi_{IM,\sigma}(n,l)\}$ has a larger dimension that the single particle space in the NC model. Indeed, here the energy level of a given total angular momentum $I\neq 0$, has a degeneracy equal to $4(2I+1)$ while for the $I=0$ case the degeneracy is equal to 2. By contrast, in the CN model the states have the degeneracy equal to $4-2\delta_{\Lambda,0}$. The difference comes from that in the CN model the states are considered in the intrinsic frame while in the present model they are considered in the laboratory frame. To simulate the distribution of fermions in the intrinsic states, for each projected I state one allows that 4 (or 2 in the case of $I=0$) electrons occupy, with equal probability, the $(2I+1)$-M states. For example the electron density for a system with $\mathcal{N}$ electrons is defined by:

$$\rho = \sum\frac{\nu(I)}{2I+1}\mid\Phi_{IM,1/2}(n,l)\mid^2,\quad \nu(I) = 4-2\delta_{I,0}, \tag{2.13}$$

where the summation is performed over all occupied states.

The model presented above was successfully used [17] to describe several essential properties of the Na clusters: magic numbers, cluster shapes, super-shell effects. In all applications presented, it was considered that the core contribute to the single particle energies only *via* the interacting terms and thereby we took $\omega_{\rm c}=0$. This assumption is adopted also in the present paper.

Two distinctive features of the present model are to be mentioned. The mean field is determined by averaging the particle-core Hamiltonian on a coherent state describing the deformed core. As a result the mean field depends on

[1] In reference [17] there is a miss-print in the expression defining the energies referring to the sign of D and the exponent of the $\left(\Omega_\perp^2 - \Omega_z^2\right)$ term multiplying F_{Il}. Numerical results correspond to the correct formula (2.12).

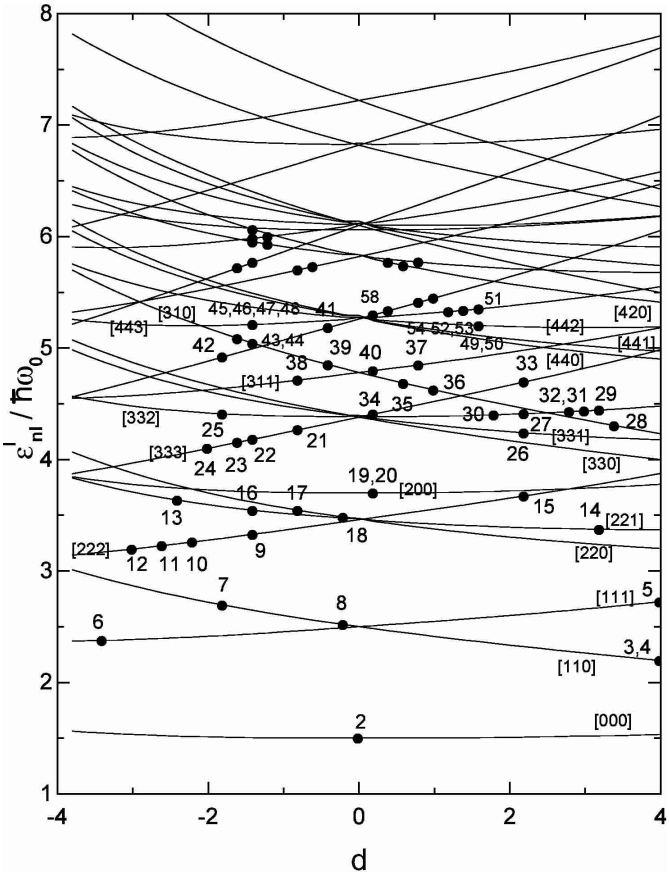

Fig. 1. The single particle energies given by equation (2.12), in units of $\hbar\omega_0$ are plotted as functions of the deformation parameter d. 33e equilibrium deformation for a system with $\mathcal{N}$ electrons is shown by black circles. The quantum number of the corresponding state $[Nl I]$ are also presented.

the core deformation. The procedure resembles the Born-Oppenheimer approximation. The core contributes to the single particle energies (see the structure of the projected states) and therefore to removing the M-degeneracy, not only by its ground state but also through its excited states. This feature simulates the cluster property saying that the distortion of single particle orbits is due to the vibration of the ionic core [20]. Higher multipoles, introduced in the mean field in reference [21], seem not to influence essentially the properties analyzed in the present paper.

In the next section we shall investigate some new properties of the Na clusters.

3 Electron density

Here we shall use the same conventions as in reference [17]. For the sake of a self standing presentation we mention them below. The units are of a.u. type ($\hbar = m_e = c = 1$). For length and energy the units are 0.53 Å and $2Ry = 27.2$ eV. The oscillator length b and energy quanta $\hbar\omega_0$ are $3\mathcal{N}^{\frac{1}{6}}$ a.u. and $0.11\mathcal{N}^{-\frac{1}{3}}$ a.u., respectively. Some of the results will be compared to the jellium model (JM) where

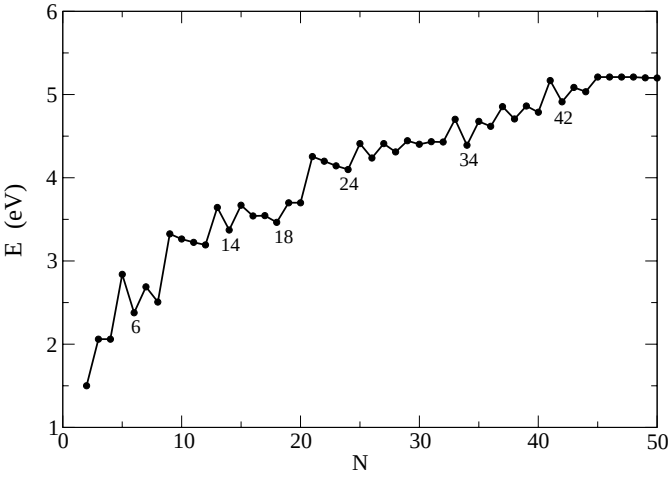

Fig. 2. The energy of the highest occupied state in $Na_{\mathcal{N}}$ is given in units of eV.

the ionic charge is uniformly distributed in a sphere of radius

$$R = r_s \mathcal{N}^{\frac{1}{3}} \tag{3.1}$$

with r_s standing for the Wigner Seits radius which for sodium clusters is about 3.93 a.u.

The single particle energies are given in Figure 1 as a function of the deformation parameter d. The energy of a cluster with $\mathcal{N}$ atoms is calculated by summing the single particle energies, corresponding to a given deformation d, for the states occupied by the $\mathcal{N}$ atoms. As in reference [17], for all clusters considered here, the parameter k from equation (2.3) was taken equal to 9.77. We shall call equilibrium deformation that value of d which minimizes the total energy of the chosen cluster. For the clusters with $\mathcal{N}$ smaller than 70, the equilibrium deformations are represented in Figure 1 by black circles. The quantum numbers $[Nl I]$ characterizing the states of energy $\epsilon^I_{nl}(d)$ are also given.

In Figure 2 we plot the energy of the last electron, represented in Figure 1 by black circles. Note that for any magic cluster $\mathcal{N}$ the last electron energy is smaller than that corresponding to the $\mathcal{N}+1$ cluster. As shown in reference [17] this determines a big peak in the second difference of the total energy of valence electrons. Our results are slightly different from those obtained with the NC model. For example the peaks associated to the minima from Figure 2 at $\mathcal{N} = 12, 24, 32$ do not exist there. Indeed they are shifted to $\mathcal{N} = 10, 26, 34$, respectively. The shell structure may also be pointed out in the plot showing the $\mathcal{N}$ dependence of the shell correction of the total energy. Indeed, this curve exhibits minima for magic values of $\mathcal{N}$. Comparing our results with those obtained by different formalisms in references [21,22] several differences are to be mentioned. While our model predicts $\mathcal{N} = 40, 186$ as magic numbers, in reference [22] one obtains instead $\mathcal{N} = 34$ and 168, respectively. Also in reference [21], the cluster $\mathcal{N} = 186$ is not predicted as magic. Another difference with reference [21] concerns the cluster

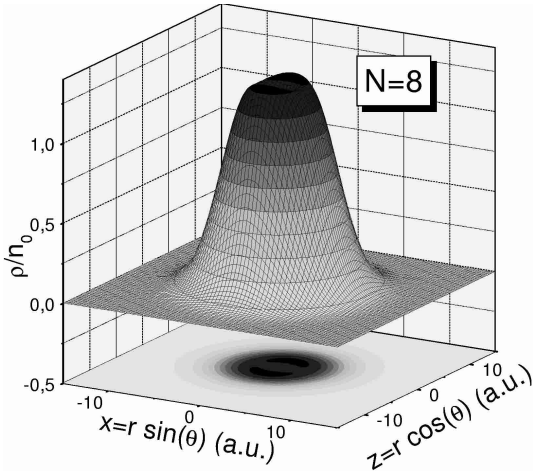

Fig. 3. The cluster density (2.13) normalized to n_0, given by equation (3.2), is plotted as a function of (x, z) for $y = 0$ for Na_8. In the plane (x, z) the equi-density contour is plotted.

with $\mathcal{N} = 292$ which is magic in our formalism while in the above quoted reference there is no magic cluster with $\mathcal{N}$ around 300. The above mentioned differences might be caused by the fact that we use a projected spherical single particle basis.

Here we want to see whether there are signatures for magic clusters revealed by the electron density. To this end we plot in Figures 3 to 10 the total density, given by equation (2.13), normalized to the density inside the jellium sphere:

$$n_0 = \left(\frac{4\pi}{3} r_s^3\right)^{-1}. \tag{3.2}$$

In the low plane of the plots we give the equi-density contour. For each magic cluster one finds indeed a distinctive feature. To begin with let us look at Na_8 where one distinguishes two maxima (Fig. 3). Note that multiplying ρ with the electron charge one obtains the charge density. The two maximal charge densities remind us of the classical rod effect saying that the charge distributed on a surface has maximum density in the place corresponding to a maximum curvature. The equi-density curves show a clusterization of the maximal density. Therefore in some small regions of the configuration space the cluster Na_8 behaves like two clusters of Na_4. As shown by Figure 4a the clusterization persists in Na_{12}.

However a new element appears there, namely the small density spot in the middle of the equi-density plot. For a better representation, the equi-density plot for Na_{12} is shown in Figure 4b in a plane seen in the perpendicular direction. Inside the black background of second highest density one remarks two distinct regions of lower densities. This feature could be interpreted by saying that Na_{12} consists of a Na_8^* core and two clusters each of them with two atoms. Note that for Na_{12} the first 8 electrons are distributed in energy levels which differ from those of Na_8, despite the fact they carry similar quantum numbers. Therefore the subsystem of 8 electrons from Na_{12} is conventionally associated to an excited cluster, Na_8^*. Usually

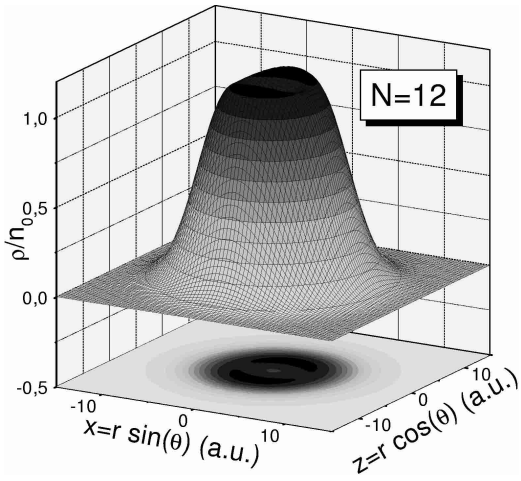

(a)

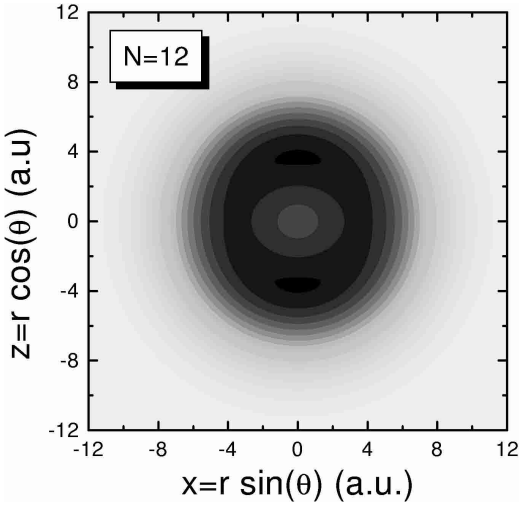

(b)

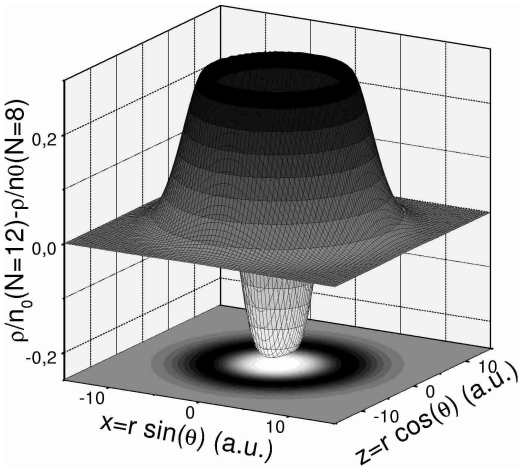

(c)

Fig. 4. (a) The same as in Figure 3 but for Na_{12}. (b) The data are the same as in (a). The equi-density plot is presented in a plane viewed in a perpendicular direction. (c) The difference of normalized densities for Na_{12} and Na_8 is shown as function of the variables (x, z) for $y = 0$. The equi-density plot is given in the plane (x, z).

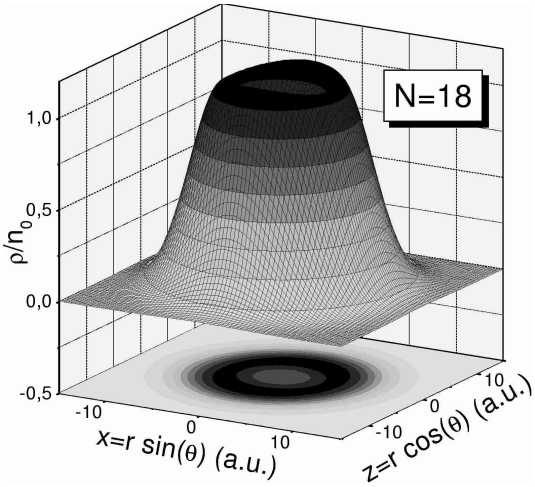

Fig. 5. The same as in Figure 3 but for Na_{18}.

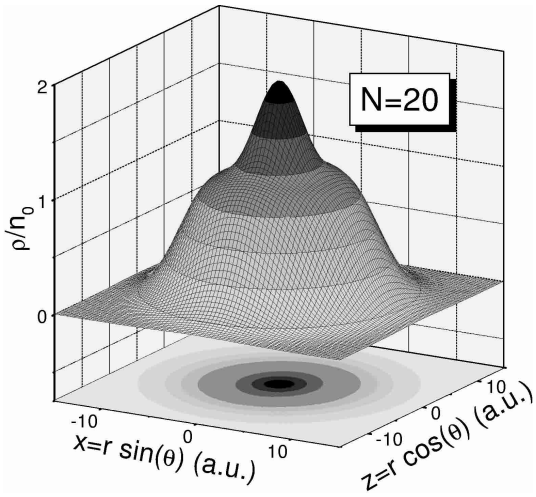

(a)

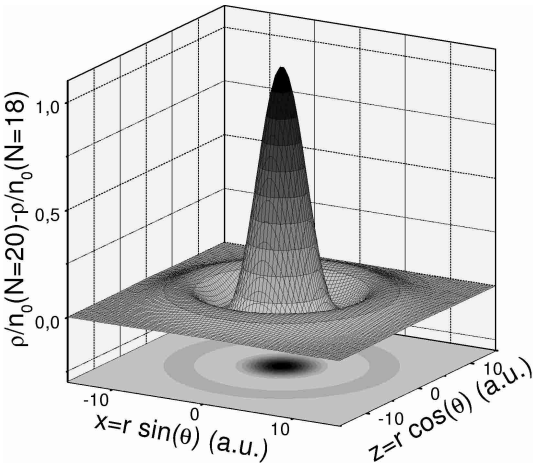

(b)

Fig. 6. (a) The same as in Figure 3 but for Na_{20}. (b) The same as in Figure 4c but for Na_{20} and Na_{18}.

the cluster shape is defined by an equi-density contour. In Figure 4b the shape of the second highest density contour is prolate while the shape of the inner contour is of oblate type. The clusterization is even more evident in Figure 4c where we plot the difference of the densities for Na_{12} and Na_8. The lowest density region from the central contour of Figure 4b correspond to the pillar under the hat of Figure 4c. The second lowest minimum is another pillar thicker than the first one and covered by the hat in its upper part. In the first two lowest density regions the density of Na_8 is larger than that of Na_{12} and that happens due to the fact that Na_{12} is deformed while Na_8 is spherical. However there is a peripheral region where Na_{12} has a density higher than that of Na_8. We interpret this "satellite" density as cluster added to Na_8. It is worth to remark the fact that the change of density color is associated to filling a major shell. Since the electron density for states of higher energy is more spread than those of the inner ones, the dark spots in Figure 4b are determined by the last four electrons which lie in the orbit [222]. Indeed, their total density is proportional to the sum of the square of the quadrupole spherical functions, *i.e.* $\sum |Y_{2m}|^2$, and exhibits two maxima for $\theta = 0$ and $\theta = \pi$. Since in the two space intervals the 4 electrons are distributed with equal probabilities one obtains the image of two dimers moving around a core, *i.e.* Na_8^*. This clustering features around the magic configurations hold also in the nuclear case for both the light [23] and heavy systems [24,25].

In Na_{18} (Fig. 5) the clusterization from the previous magic cluster (8) disappeared. The lower plane curve shows that the cluster is "empty" in the central part. The density increases with the radius, reaches a maximum, and then decreases again. Na_{20} exhibits also a clusterization. Indeed, there exists a central peak which makes the cluster center having the maximum density. The clusterization for Na_{20} can be better appreciated in Figure 6b where the corresponding density was normalized to that for Na_{18}. The last two electrons are placed in the state [200] and produce in Figure 6b, the dark ring as well as the central spot.

Closing the major shell characterized by $N = 3$, an interesting phenomenon happens. The cluster Na_{32} is the first magic cluster which is deformed. Indeed, Figure 1 shows that above the energy level occupied by the last electron there is an energy gap with no level inside. The magic character of Na_{32} is also proved by the plot of the second difference of the total energy, shown in Figure 3b of reference [17]. As shown in Figure 7, this cluster exhibits a high density concentrated in a small area around origin, which decreases quickly to the value $\rho/n_0 = 0.75$. This value is met in a huge circular zone and then the density goes rapidly to zero. The unusual large circular zone is, in fact, a signature for this deformed cluster. Adding two atoms to Na_{32} one obtains a spherical magic cluster, whose density behaves qualitatively different from what we see in Na_{32}. Indeed in Figure 8, for the first time, we have a skin structure, *i.e.* the density is maximum in the central part, it decreases and reaches a minimum value in a circular zone, the "empty" part, and then increases again

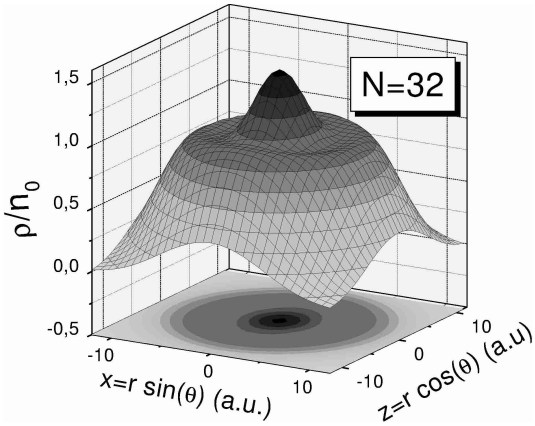

Fig. 7. The same as in Figure 3 but for Na_{32}.

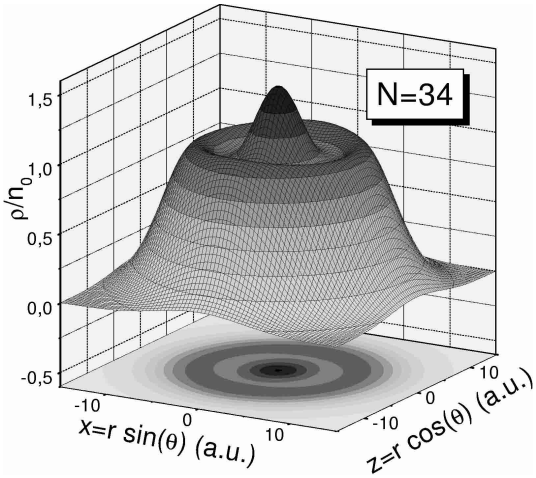

Fig. 8. The same as in Figure 3 but for Na_{34}.

reaching a maximum value followed by a quick decrease to a vanishing density. We recognize easily a chestnut structure. Clearly this is also a cluster structure since the core and the skin are two pieces of disconnected matter.

The skin structure disappears for Na_{40} shown in Figure 9, where two maxima show up. The maxima seen in Na_{40} are less evident in Na_{42} (see Fig. 10a). The relative density of Na_{42} and Na_{40}, plotted in Figure 10b, points out the two maxima discussed before as well as the outer electrons orbiting around the core Na_{40}. These maxima, though less pronounced, resemble those of Na_8, as shown in Figures 11a and 11b. Comparing the plots from Figures 7 and 9, two features are to be mentioned. The region with density $\rho/n_0 \leq 0.5$ is more narrow in the case of Na_{40}. The main contribution of the last 8 electrons is to augment the density above the plateau with $\rho/n_0 = 0.75$ in Figure 7 and change the shape from deformed to spherical. Therefore the additional 8 electrons are added in a compact manner to the central region. In this respect this situation is different from what was mentioned before for Na_{12}, namely the outer electrons contribute mainly to the internal part rather than to the peripheral region. Thus here the clusterization on the density surface does

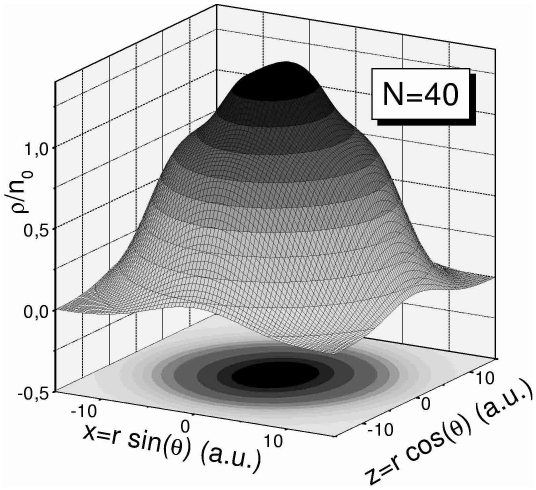

Fig. 9. The same as in Figure 3 but for Na_{40}.

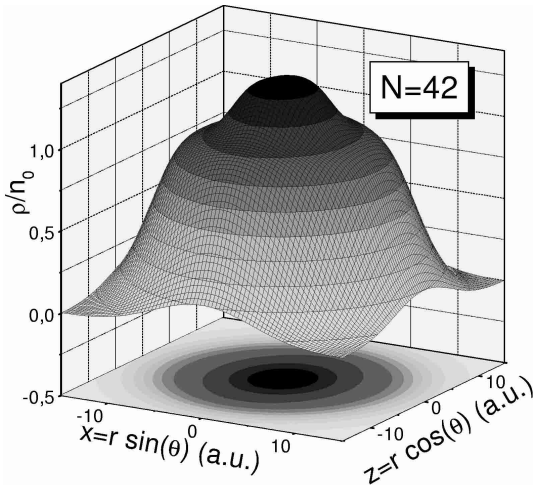

(a)

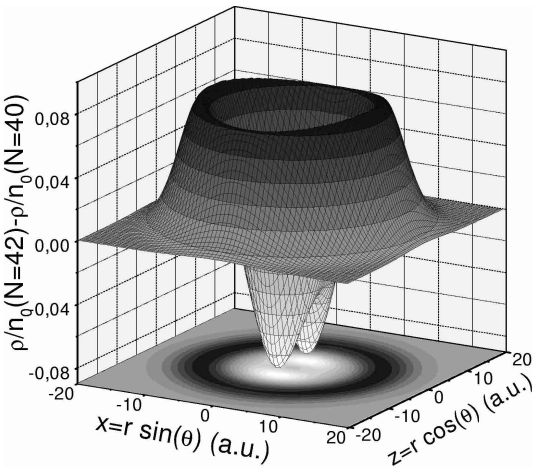

(b)

Fig. 10. (a) The same as in Figure 3 but for Na_{42}. (b) The same as in Figure 4c but for Na_{42} and Na_{40}.

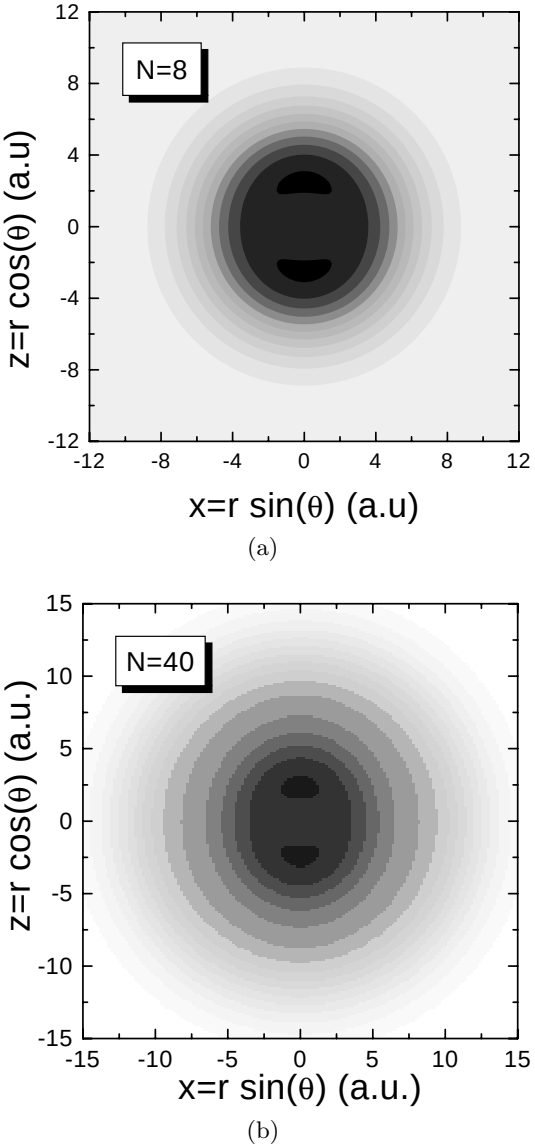

Fig. 11. (a) The same as in Figure 4b but for Na_8. (b) The same as in Figure 11a but for Na_{40}.

not correspond to a clusterization in the configuration space. However, the two spots of highest density give rise, in the three dimensional space (X, Y, Z), to two disconnected regions of the same density which is consistent to the usual meaning of clusterization. Thus, one could say that the core of Na_{40} exhibits a cluster structure with a component similar to Na_8. In fact this suggests the Na_{40} might be tentatively viewed as formed out of two clusters Na_{32}^* and Na_8^*. Here Na_{32}^* denotes the cluster with the electrons occupying the same single particle states as for Na_{32} but for vanishing deformation. The excited cluster Na_8 corresponds to the last 8 electrons distributed to the states [333] (2), [310] (2) and [311] (4). By promoting the electrons from the major shell $N = 3$ to states of the major shell $N = 4$, the magic cluster may exhibit negative parity collective states. Since Na_{40} is spherical magic, the octupole states are expected to be high in energy and of a vibrational nature. Therefore in our as well as in the CN models, the ground state of Na_{40} has good reflection symmetry which is at variance with the predictions of references [26,27] saying that this cluster has a ground state with an octupole deformation. From the study of nuclear systems it is well-known that the static octupole deformation is favored by the quadrupole deformation. Indeed, due to lifting the "m" degeneracy, the single particle states of positive and negative parity come closer to each other and thus their interaction may produce a stable octupole deformed ground state [28,29]. Concluding, an octupole deformation is usually thought as possible for quadrupole deformed systems. Hitherto convincing evidence that Na_{40} has quadrupole deformation is however missing. Due to these arguments we believe that even in the case the mean field would contain an octupole term the cluster does not exhibit a static octupole deformation.

Concluding the above analysis one may say that we identified clusters of various structures: full or empty in the center, skin like (or chestnut), clusterized. Without any exception the magic clusters exhibit a certain type of clusterization. Moreover their highest density is met in the central part. As for the non-magic clusters, the electron density in the central area is smaller (or higher) than that in the peripheral part depending on whether the number of electrons filling odd parity states is larger (or less) than the number of electrons from even parity states. In the present paper the notion of clusterization has a rich content being a manifestation of the shell structure. Indeed there are various types of clusterization, each of types acquiring a distinct definition: (a) as disconnected regions of the configuration space limited by surfaces of constant density. Moreover the components are exterior to each other. This was the case of Na_8, Na_{12} and Na_{40}. (b) Disconnected regions covered by surfaces of different constant densities, exhibiting a chestnut structure. This is the case of Na_{34}. (c) A few electrons moving around a core of nearly constant density, as a distinct entity. This is the case of Na_{42}. (d) An usual shell structure, where the shell is defined as a set of points in the configuration space characterized by the same density, with a density varying smoothly from one shell to another.

The cluster shape variation, with the number of electrons was also studied in reference [14] through the so-called ultimate jellium model. The authors of this reference also noticed a sub-cluster structure of the light magic clusters. Moreover, they identified for Na_{20} an isomer state which is "empty" in the center. In contradistinction to that situation, the present formalism predicts a ground state for Na_{18} having this property. This is a strong support for the assertion that the angular momentum projection may modify the structure of the ground state.

According to Figure 1 the clusters with $\mathcal{N} = 5, 14, 15$ have a prolate shape, while in the CN model they are of an oblate shape. Our predictions for these clusters are similar with those of reference [30], obtained in a local spin-density approximation formalism. Concerning the shape of Na_{14}, the result of the present paper is supported also

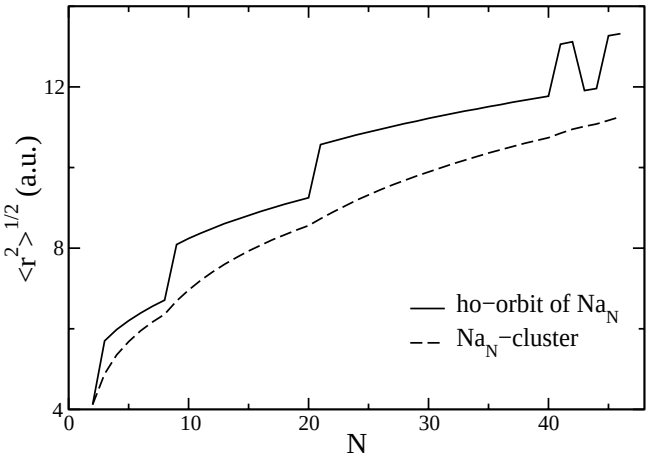

Fig. 12. The r.m.s. values for the cluster $Na_{\mathcal{N}}$ (dashed line), defined by equation (4.1) and for the highest occupied (ho) state in $Na_{\mathcal{N}}$, defined by equation (4.2) (full line), are given as function of the number of atoms.

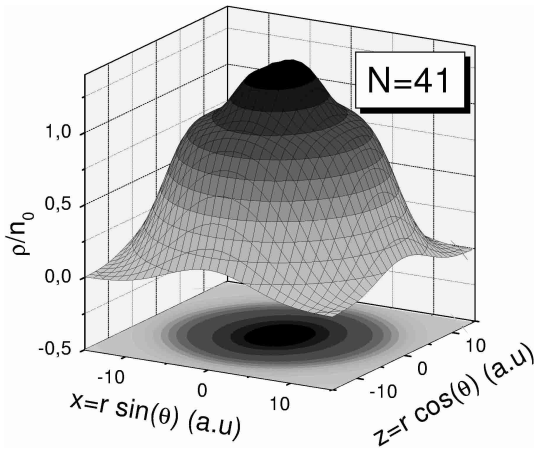

Fig. 13. The same as in Figure 9 but for Na_{41}.

by the photo-absorption data [31] showing the plasmon-resonance splitting. We stress, again, that the projected spherical single particle basis is causing these variances with the CN model. The specific structure of the clusters analyzed has, certainly, an echo in their response to the interaction with an electromagnetic field.

4 Cluster spatial extension

In reference [18] it was pointed out a striking similarity between the behaviors of nuclear and cluster systems. In fact this is the argument which supports best various attempts to extend formalisms tested for nuclear systems to cluster physics. One of the hottest subjects of nuclear physics, at present, concerns the halo structure of some light nuclei [32,33]. The halo structure in nuclei, is not a global property but characterizes the last nucleons in the system. One of the most studied cases is that of ^{11}Li where the last two neutrons have a large spatial extension and a weak binding energy. The spatial spreading is due to the fact that the last neutrons stay in the $2s_{1/2}$ state, which is favored with respect to the state $1p_{1/2}$ due to the tensorial force which is increased by the large $N-Z$ asymmetry.

Here we address the problem whether such a structure might be seen also in sodium clusters. Of course here we don't have an $N-Z$ asymmetry effect since we have only one type of fermions with a unique charge. However in the higher part of the spectrum many level crossings appear as shown in Figure 1. A measure for the spatial extension is the r.m.s. value defined by

$$\langle r^2\rangle_{\mathcal{N}}^{1/2} = \left[\frac{1}{\mathcal{N}}\int r^2\rho\,\mathrm{d}^3r\right]^{1/2}, \qquad (4.1)$$

with the density function given by equation (2.13). For the last electron, the r.m.s. value is defined by

$$\langle r^2\rangle_{\rm ho}^{1/2} = \left[\int r^2|\Phi_{IM;1/2}(nl;d)|^2\,\mathrm{d}^3r\right]^{1/2}, \qquad (4.2)$$

where only the density for the highest occupied level (ho) is considered. From Figure 12 we see that while the r.m.s. value for the cluster $Na_{\mathcal{N}}$ has a smooth behavior with $\mathcal{N}$ the r.m.s. value for the last electron has a discontinuity at the magic numbers 8, 20, 40 and a peak for $\mathcal{N}=41,42$. As shown in Figure 2, the corresponding odd clusters 9, 21, 41, are characterized by minimal ionization energy for the last electron. A particular interest deserves the cluster Na_{41} since according to Figure 12 it is followed by a jump back of the r.m.s value at Na_{43}. Inspecting Figure 1 one sees that the level inversion mentioned above takes place indeed for the case of Na_{42}. Indeed the last two electrons of Na_{42} do not occupy the level $[NlI]=[310]$, as it happens for Na_{43} and Na_{44}, but the state [444] descending from the upper major shell. The analogy with the nuclear case is only partial since here the intruder state is of high angular momentum ($l=4$) and therefore one obtains only a moderate large extension. On the other hand the last electron energy in Na_{41} is maximum with respect to that of the neighboring clusters (see Fig. 2), which means that this odd cluster is characterized by a minimum ionization energy. By contrast in the nuclear case, the spatial spreading is a combined effect of a level crossing and a low value of the orbital angular momentum. Comparing the axes of the last large equi-density contours ($\rho/n_0\approx 0.5$) we see that the longer axis of Na_{41}, Figure 13, is sensibly larger (with about 2 a.u.) than that for Na_{40}, given in Figure 9. From Figure 2 one obtains that the r.m.s. for Na_{41} is about 1.1 a.u. larger than for the neighboring clusters with $\mathcal{N}=40,43,44$. Summarizing, in the present description two interesting features were pointed out, caused by the crossing of levels belonging to different major shells. The cluster Na_{42} has the last electron strongly bound and its orbit is largely spread due to the fact that the corresponding deformation is large. The odd system Na_{41} has the last electron minimally bound, or in other words it is characterized by a minimum ionization energy, and moreover the orbit of the last electron has a large r.m.s. value.

Concluding, despite the fact that the last electron in Na_{41} moves with a large orbital angular momentum, $l=4$, the behavior of ionisation energy and the r.m.s

value against the variation of the total number of atoms resembles the properties of nuclear systems necessary for a halo structure.

It is an open question whether this property influences in a visible manner the global behavior of Na_{41}.

5 Static polarizability and plasmon frequency

At the classical level the polarizability of a metallic sphere of radius R is defined as follows. Suppose the sphere is placed in a uniform electric field $\mathbf{E}$. Then the sphere behaves as an electric dipole $\mathbf{P}$ parallel to $\mathbf{E}$. The ratio of the magnitudes of the two vectors P/E is called polarizability. The dipole appears as a reaction of the metallic sphere to the external field, the charge inside the sphere being slightly displaced so that the generated field cancels the external one, inside the sphere. For a metallic sphere of radius R the polarizability is equal to R^3. For a metallic cluster with the jellium sphere of radius R, this is referred to as the classical value of polarizability. The experimental data for small sodium cluster (up to 40 atoms per cluster) showed that the polarizability exceeds the classical value by 60–80% but it goes to the bulk value when the number of constituents is increased, [34–36]. It seems that the electrons spillout of the boundary of the positive background screens the external field which results in having a polarizability increased from R^3 to $(R+\delta)^3$. The numerical calculations with density-functional method predict polarizabilities larger than the classical values but still 20% under the experimental data [37–40]. Having in mind the classical picture, the structure of the charge density function is determining the position of the center of mass of the spillout electrons. In this respect the description of the static polarizability is a challenge for any microscopic model. Moreover, since the external field induces a dipole moment *via* polarization of the electronic charge, it may excite a dipole giant state. Therefore there is a direct connection between polarizability and the plasmon frequency which is expressed by the dipole sum rule [4,41–45]. Indeed, the polarizability is twice the inverse energy-weighted sum rule while the squared plasmon energy, for a spherical system, is given by the ratio of the energy and the inverse energy sum rules. The classical result for the plasmon energy was calculated first by Mie [46], long time ago, and is determined by the potential inside a uniformly charged metallic sphere which, up to an additive constant, is given by:

$$\frac{2\pi\rho_j}{3}r^2 = \frac{1}{2}m_{\rm e}\omega_{\rm Mie}^2 r^2, \tag{5.1}$$

where ρ_j denotes the jellium density. This yields immediately for the Mie frequency the expression:

$$\omega_{\rm Mie} = r_{\rm s}^{-3/2}[\text{a.u.}]. \tag{5.2}$$

Considering the Mie frequency in the above mentioned equation relating the plasmon energy and the static polarizability, one obtains for the static polarizability of a metal-sphere of radius R, the following expression:

$$\alpha_0 = R^3. \tag{5.3}$$

Quantum mechanical effects determine corrections to the classical results for plasmon energy and polarizabilities. The electron density is not going sharply to zero at the cluster surface but reduces gradually at the surface and moreover extends significantly beyond to jellium edge. The spillout electrons produce a screening effect against external fields which results in changing the classical result for polarizability to:

$$\alpha = (R+\delta)^3. \tag{5.4}$$

The radius shift δ can be expressed in terms of the fraction of the total number of electrons which are spilled out the jellium sphere and the final result for the static polarizability reads:

$$\alpha = R^3\left(1+\frac{\mathcal{N}_{\rm sp}}{\mathcal{N}}\right), \tag{5.5}$$

where $\mathcal{N}_{\rm sp}$ denotes the number of spilled out electrons and is given by:

$$\mathcal{N}_{\rm sp} = \int_{r>R}\rho\,{\rm d}^3r. \tag{5.6}$$

The static polarizability given above approximate quite well the result predicted by the inverse-energy weighted sum rule:

$$\alpha = R^3\left(1-\frac{\mathcal{N}_{\rm sp}}{\mathcal{N}}\right)^{-1}. \tag{5.7}$$

Although the static polarizability given by (5.5) is formally identical to that given earlier in the literature [41], there is, however, a new feature in the present paper, consisting in that the electron density is determined by the projected spherical single particle basis.

The energies of the dipole resonances corresponding to the three independent directions can be obtained within the RPA (random phase approximation) formalism as coherent superposition of the particle hole excitations. However, it is much easier to calculate these energies using classical arguments. Indeed the total work performed by displacing the charges from the points $\mathbf{r}$ to $\mathbf{r}+\Delta x\mathbf{i}+\Delta y\mathbf{j}+\Delta z\mathbf{k}$ can be written as the sum of three string potential energies. The result for the plasmon energy corresponding to the vibration along the direction "i" is:

$$\hbar\omega_i = \left[-\frac{e\hbar^2}{\mathcal{N}m_{\rm e}}\int {\rm d}^3r V_{\rm bg}(\mathbf{r})\frac{\partial^2}{\partial x_i^2}\rho(\mathbf{r})\right]^{1/2} \tag{5.8}$$

where $V_{\rm bg}$ denotes the background potential created by the ionic core. This potential energy is obtained following the arguments already given for the deformed mean field of single particle motion. For example the potential energy corresponding to the single particle basis used in the present paper, is obtained by averaging the right hand side of equation (2.1) on the coherent state (2.5) and leaving out the terms depending on single particle linear momentum. The final expression for the background potential

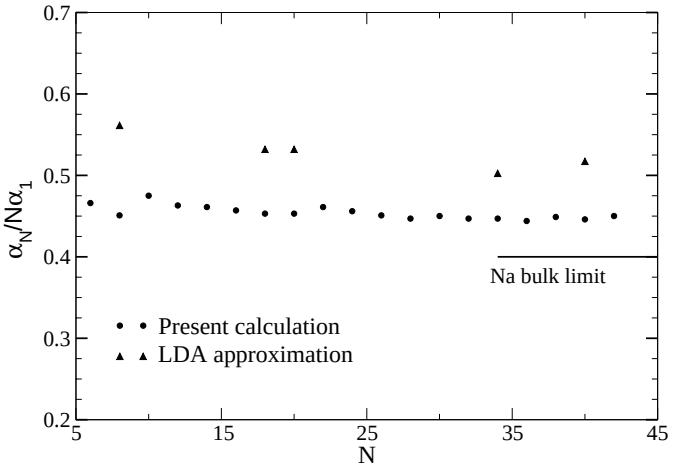

Fig. 14. The static polarizabilities predicted by the present work (black circles) are compared with those given in reference [27] with a LDA approach and the bulk limit.

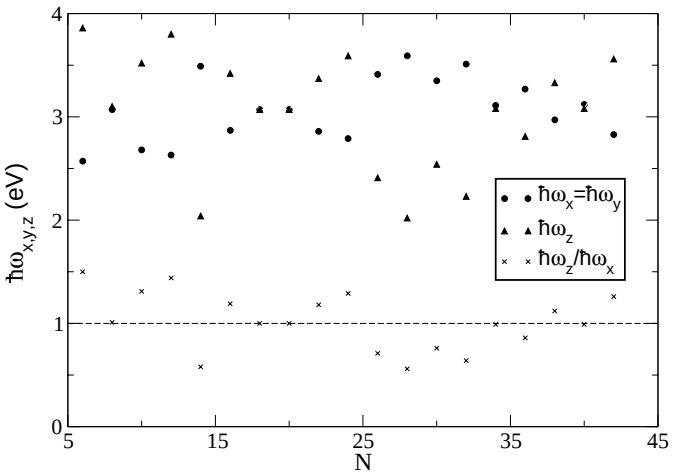

Fig. 15. The plasmon energies for x, y and z axes are given in units of eV. They are calculated with equation (5.8).

obtained by deforming the spherical Coulomb potential, which defines $\omega_{\rm Mie}$ by means of equation (5.1), is:

$$V_{\rm bg}(\mathbf{r}) = V_0 + m_{\rm e}\omega_{\rm Mie}^2 \times \left[\left(\frac{1}{2} + \frac{4d^2+5}{8\pi k^2}\right) r^2 - \frac{d\sqrt{2}}{k} r^2 Y_{20}(\theta,\phi)\right]. \quad (5.9)$$

For a compact writing we have used the notation $(x_1, x_2, x_3) = (x, y, z)$. The first term in equation (5.9) is a negative constant chosen so that for $d = 0$ the potential vanishes outside the jellium sphere. The difference between the $\mathcal{N}$ dependences of oscillator frequencies ω_0 and $\omega_{\rm Mie}$ is discussed in detail in reference [47]. The second frequency characterizes a surface oscillation caused by a long range interaction, *i.e.* Coulomb force, while the first frequency may induce a volume plasmon oscillation.

Performing twice an integration by parts in equation (5.9) and using the properties of $V_{\rm bg}$ and $\partial\rho/\partial x_i$ for $r = 0$ and $r = R$, one finds the final expression for the plasmon frequency:

$$\omega_i = \omega_{\rm Mie}\left[f_i \frac{\mathcal{N}_{\rm ins}}{\mathcal{N}}\right]^{1/2} \text{[a.u.]},\ i = x, y, z \quad (5.10)$$

where $\mathcal{N}_{\rm ins}$ denotes the number of electrons inside the jellium sphere and the factors f_i are:

$$f_i = \frac{\partial^2 V_{\rm bg}}{\partial x_i^2}\,. \quad (5.11)$$

Note that for spherical clusters the coefficients f_i, in equation (5.10), are all equal to unity and the corresponding plasmon energy is identical to that predicted by the sum rule approach. Since the factor accompanying $\omega_{\rm Mie}$ in equation (5.10) is less than unity, the classical plasmon is red shifted.

Our numerical calculations, shown in Figure 14, include clusters with $\mathcal{N}$ up to 42. The polarizability is obtained from equation (5.5). In order to indicate the $\mathcal{N}$ dependence we introduce a lower index for it. For a better presentation we normalize the predicted values to $\mathcal{N}\alpha_1$ where α_1 denotes the polarizability of the sodium atom and has the value of 159 a.u. [48]. Our results are about 10% lower than the prediction of the local density approximation (LDA) [38] and about the same amount above the bulk limit.

The plasmon energies are presented in Figure 15. Since the mean field has axial symmetry, two of the plasmon energies are equal to each other. We also plot the ratio ω_z/ω_x.This ratio is equal to one for spherical, under-unity for prolate, and over-unity for oblate clusters. Of course the energy splittings depend on the magnitude of the deformation parameter d. The larger d, the larger the energy split. If one defines and average energy for each cluster:

$$\overline{\omega} = \frac{1}{3}(\omega_x + \omega_y + \omega_z). \quad (5.12)$$

This quantity is equal to about 3 eV for all clusters considered here. The largest value is 3.11 eV, reached for Na_{40}, while Na_{10} has the lowest average energy, equal to 2.96 eV. The present results for spherical clusters Na_8, Na_{20}, Na_{40} are larger than those reported by Kresin in reference [49] and obtained with the statistical Thomas-Fermi approach. The results there, for the three clusters are 2.53, 2.67 and 2.77 eV, respectively. The results presented here for light clusters are similar to those obtained through a local RPA approach in reference [50], where the centroid energy is about 3 eV.

The predicted energies in our approach are higher than the energy of the RPA collective state. This happens since while in our case all strength is concentrated in one state, in the RPA formalism the dipole strength is distributed among several states. For deformed clusters, the RPA approach using the CN single particle basis predicts states with $K = 1$ where K denotes the eigenvalue of the angular momentum projection on the symmetry axis. However, in the predicted RPA state the angular momentum has not a definite value. Due to this fact, the distribution of the

dipole strength is affected by errors. In order to provide an accurate description of the dipole E1 transitions from ground to the RPA states, the use of states of good angular momentum is necessary. A possible solution for this problem is offered by the present paper where a projected spherical single particle basis is defined. An extensive RPA description based on the single particle space defined in reference [17] and the present paper, is under work and the results will be published in a forthcoming paper.

For axial symmetric clusters the plasmon energies shown in Figure 15 agree very well with the corresponding predictions of the ultimate jellium model [14]. Among light clusters with an even number of components two cases of non-axial shapes were identified. These are Na_{12} and Na_{16}. By inspecting Figure 4b for Na_{12}, one may attempt to associate the three plasmon frequencies to the three regions characterized by the three distinct equi-density contours. Indeed, for a slightly asymmetric mean field the inner region may accommodate a distinct shape and exhibits a motion with a specific frequency. In an RPA formalism, the configurations contributing most to the three regions may build up coherently the three modes of the deformed system. Actually this is only one possible effect caused by the complex structure of the density function shown in Figures 3–10b.

6 Conclusions

The projected spherical single particle basis, introduced by one of the present authors (A.A.R.) in a previous publication, is used to investigate new properties of sodium clusters. The main results presented in the previous sections can be summarized as follows.

A systematic analysis of the valence electron density is performed. The modification of the density function as well as of the equi-density contour plots, with the number of atoms is pointed out. Several interesting structures for the cluster density are found. Features as, high density or "empty" (*i.e.* low density) in the central part, clusterization of small clusters inside the big cluster, skin (or chestnut) structures are identified for clusters with less than 45 atoms. All magic clusters exhibit a certain kind of clusterization structure which may be seen either in the configuration space as disconnected regions closed by a surface of constant density respectively, or some disjunct areas on the the density plotted in the variables (X, Z).

The predicted shapes are in good agreement with other theoretical results obtained with different formalisms. However, several discrepancies are pointed out. In the case of Na_{14} the existent data [31] confirm our prediction. The spatial distribution of the electron density may generate independent harmonic modes corresponding to distinct deformation degrees of freedom.

Guided by the analogy with the nucleon systems we searched for a halo structure in atomic clusters. It seems that we found one in the small cluster region. Indeed, Na_{41} has the specific properties of a halo structure, *i.e.* the last electron has a large spreading comparing its size to that of the neighboring clusters, and also it is weakly bound. As shown in Figure 10b, Na_{42} consists of two atoms moving around a core (Na_{40}) which has a cluster structure of two smaller sub-cores of magic clusters Na_{32} and Na_8. Such a structure might be seen through an induced fragmentation process for Na_{42}.

The static polarizability and plasmon energies have been calculated. Our results for polarizabilities are above the bulk limit by a 10%, and by about the same amount below the predictions of LDA approach. The deviation from experimental data are of the order of 30%. This is to be expected in the classical scheme used here, and can be improved with RPA calculations.

The plasmon energies were calculated with the formula (5.10). For spherical clusters there is only one state while departing from the magic cluster the state split into two parts one consisting in two degenerate states of energy $\omega_x = \omega_y$ and another one of energy ω_z. The split increases with $\mathcal{N}$, meets the maximum value at the middle of the distance between the two consecutive magic clusters and then decreases to zero at the next magic cluster. The ordering of the two energies depends on the cluster shape. For prolate clusters $\omega_z \leq \omega_x$ while for oblate clusters the ordering is changed. The strong dependence on the number of atoms, for the the plasmon energies is caused by the modification of the charge density, described in Section 3, when the number of atoms is increased. Similar calculations have been performed with the ultimate jellium model in reference [14]. Apart from the fact that they identify a triaxial shape in Na_{12} and Na_{16} our results agree quite well.

Although the experimental data are obtained in the laboratory frame, where the rotational symmetry is present, the CN model is able to nicely reproduce many data. In such cases the K-components of the considered observable have such a distribution that one K-component is by far prevailing over the remaining ones. However if the mixture has not a privileged K-component the results in the intrinsic and laboratory frame are different from each other. Obviously in the former cases one expects that the present paper and CN predictions are close to each other, while in the later case they are different. As a matter of fact, throughout this paper we gave several examples belonging either to the first or to the second class of properties.

In a forthcoming publication we shall exploit the quality of our single particle basis of having good angular momentum, and perform an RPA-particle-hole calculations for the giant dipole resonance.

As a final conclusion one may say that the projected single particle basis seems to be suitable for describing the main properties of the atomic clusters.

This work was supported by CNCSIS (Romania) under the contract A918/2001.

References

1. W.D. Knight, K. Clemenger, W.A. de Heer, W.A. Saunders, M.Y. Chou, M.L. Cohen, Phys. Rev. Lett. **52**, 2141 (1984).

2. G. Galli, Parrinello, in Comp. Sim. in Material Science, NATO ASI E: Applied Sciences, edited by M. Meyer, V. Pontikis (Kluwer Academic, Dordrecht), p. 283, Vol. 205.
3. W.A. de Heer, Rev. Mod. Phys. **65**, 611 (1993).
4. M. Brack, Rev. Mod. Phys. **65**, 677 (1993).
5. M. Cini, J. Catal. **37**, 187 (1975).
6. V. Bonačič-Koutečky, P. Fantuccci, J. Koutečky, Phys. Rev. B **37**, 4369 (1988).
7. W. Kohn, L.J. Sham, Phys. Rev. A **140**, 1133 (1965).
8. J.L. Martins, J. Buttet, R. Cae, Phys. Rev. B **31**, 1884 (1985).
9. D.E. Beck, Solid State Commun. **49**, 381 (1984).
10. H. Nishioka, K. Hansen, B. Mottelson, Phys. Rev. B **42**, 9377 (1990).
11. M.Y. Chou, M.L. Cohen, Solid State Commun. **52**, 645 (1984).
12. C. Yannouleas, R.A. Broglia, Phys. Rev. A **44**, 5793 (1991).
13. C. Yannouleas, Uzi Landman, Phys. Rev. B **51**, 1902 (1995).
14. M. Koskinen, P.O. Lipas, M. Manninen, Z. Phys. D **35**, 285 (1995).
15. K. Clemenger, Phys. Rev. B **32**, 1359 (1985).
16. S.G. Nilsson, K. Dan. Vidensk. Selsk. i Mat. Fys. Medd. **29**, No. 16 (1955).
17. A.A. Raduta, Ad.R. Raduta, Al.H. Raduta, Phys. Rev. B **59**, 8209 (1999).
18. M. Koskinen, P.O. Lipas, M. Manninen, Nucl. Phys. A **591**, 421 (1995).
19. A. Rigo, M. Casas, F. Garcias, E. Moya de Guerra, P. Sarriguren, Phys. Rev. B **57**, 11943 (1998).
20. H.A. Jahn, E. Teller, Proc. R. Soc. Lond. A **161**, 220 (1937).
21. S. Frauendorf, V.V. Pashkevich, Z. Phys. D **26**, 598 (1993).
22. O. Genzen, M. Brack, Phys. Rev. Lett. **67**, 3286 (1991).
23. D.M. Brink, H. Friedrich, A. Weguiny, C.W. Wong, Phys. Lett. B **33**, 143 (1970).
24. A.A. Raduta, D.S. Delion, N. Lo Iudice, Phys. Rev. C **44**, 1929 (1991).
25. A. Sandulescu, D.N. Poenaru, W. Greiner, Sov. J. Part. Nucl. **11**, 528 (1980).
26. J. Kolehmainen, M. Koskinen, H. Hakkinen, M. Manninen, S. Reimann, Chec. J. Phys. **48**, 679 (1999).
27. S.M. Reimann, S.M. Reiman, M. Koskinen, H. Hakkinen, P.E. Lindelof, M. Manninen, Phys. Rev. B **56**, 12147 (1997).
28. A.A. Raduta, Al.H. Raduta, A. Faerssler, Phys. Rev. C **55**, 1747 (1997).
29. A.A. Raduta, A. Faessler, R.K. Sheline, Phys. Rev. C **57**, 1512 (1998).
30. W. Ekardt, Phys. Rev. B **31**, 6360 (1985); B **32**, 1961 (1985).
31. J. Borggreen, P. Chowndhury, N. Kebaili, L. Lundsberg-Nielsen, K. Lutzenkirhen, M.B. Nielsen, J. Pedersen, H.D. Rasmussen, Phys. Rev. B **48**, 17507 (1993).
32. I. Tanihata *et al.*, Phys. Lett. B **160**, 380 (1985).
33. P.G. Hansen, A.S. Jensen, B. Jonson, Annu. Rev. Nucl. Part. Sci. **45**, 591 (1995).
34. W.D. Knight, K. Clemenger, W.A. de Heer, W.A. Saunders, Phys. Rev. B **31**, 2539 (1985).
35. W.D. Knight, W.A. de Heer, K. Clemenger, W.A. Saunders, Solid State Commun. **53**, 445 (1985).
36. W.A. de Heer, K. Selby, V. Kresin, J. Masui, M. Vollmer, A. Chatelain, W. Knight, Phys. Rev. Lett. **59**, 1805 (1987).
37. I. Moullet, J.L. Martins, F. Reuse, J. Buttet, Phys. Rev. B **42**, 11598 (1990).
38. W. Eckardt, Phys. Rev. B **29**, 1558 (1984).
39. D.E. Beck, Phys. Rev. B **30**, 6935 (1984).
40. M.J. Puska, R.M. Nieminen, M. Manninen, Phys. Rev. B **31**, 3486 (1985).
41. N. van Giai, Progr. Theor. Phys. Suppl. **124**, 1 (1996).
42. G. Bertsch, W. Eckardt, Phys. Rev. B **32**, 7659 (1985).
43. V. Kresin, Phys. Rep. **220**, 1 (1992).
44. E. Liparini, S. Stringari, Z. Phys. D **18**, 193 (1991).
45. C. Guet, Comm. At. Mol. Phys. **31**, 305 (1995).
46. G. Mie, Ann. Phys. (Lpg) **25**, 377 (1908).
47. P.G. Reinhard, S. Weisgerber, O. Genzen, M. Brack, Z. Phys. A **349**, 219 (1994).
48. R.W. Molet, H.L. Schwarz, T.M. Miller, B. Bederson, Phys. Rev. A **10**, 1131 (1974).
49. V. Kresin, Phys. Rev. B **40**, 12507 (1989).
50. P.G. Reinhard, M. Brack, O. Genzken, Phys. Rev. A **41**, 5568 (1990).